6th European Conference on Computational Mechanics (ECCM 6)
7th European Conference on Computational Fluid Dynamics (ECFD 7)
1115 June 2018, Glasgow, UK

EFFECT OF WALL-STRESS MODEL AND MESH-CELL TOPOLOGY ON THE PREDICTIVE ACCURACY OF LES OF TURBULENT BOUNDARY LAYER FLOWS

TIMOFEY MUKHA[1], MATTIAS JOHANSSON[2] AND MATTIAS LIEFVENDAHL[1,2]

[1] Uppsala University, Sweden
PO Box 256, SE-751 05 Uppsala, Sweden
timofey.mukha@it.uu.se, www.uu.se.

[2] Swedish Defence Research Agency (FOI)
SE-164 90 Stockholm, Sweden
mattias.liefvendahl@foi.se, mattias.johansson@foi.se, www.foi.se.

Key words: Large Eddy Simulation, Wall Modelling, Turbulent Boundary Layer, Unstructured Mesh

Abstract. Results are reported from wall-modelled large eddy simulations (WMLES) of a zero pressure gradient flat-plate turbulent boundary layer (TBL) flow performed using unstructured computational meshes. In particular, two meshes are considered: a hex-dominant and a polyhedral. The resolution of the meshes is kept constant with respect to the local thickness of the TBL. The WMLES predictions are evaluated by comparison with reference data from direct numerical simulation (DNS) and semi-empirical expressions for the development of integral quantities along the TBL. Good agreement is observed for the skin friction coefficient, mean streamwise velocity and the Reynolds stresses. Also, the influence of the location of the sampling (matching) point of the employed algebraic wall-stress model is investigated. It is found that moving the sampling point to the third consecutive off-the-wall cell centre leads to a significant improvement in the prediction of the mean wall shear stress, as opposed to sampling for the wall-adjacent cell.

1 INTRODUCTION

The number of applications of LES, and other scale-resolving approaches, such as detached eddy simulation and different forms of RANS-LES hybrids, is steadily increasing in applications [26, 25]. Wall-resolving LES (WRLES), in which the energetic flow structures in the inner part of the TBL are resolved, puts excessive requirements on the mesh resolution, see e.g. [27, 13]. The fundamental motivation for WMLES is alleviating these requirements by modelling the effect of the inner region of the TBL, and only resolving the energetic structures in its outer region [21, 11].

A large number of works on WMLES of canonical flows has been published, in particular, on fully-developed turbulent channel flow, see e.g. [18, 20, 22]. Somewhat surprisingly,

the number of applications of WMLES to more complex geometries is quite limited [4]. Examples of studies that have been reported in the literature include simulations of airfoils at large angle of attack [5, 3, 19], and of flow around a car [1].

In the present paper, a complete WMLES approach, also applicable to complex geometries, is described and evaluated in terms of its predictive accuracy for a zero pressure gradient TBL over a flat plate. The main feature of the approach is to adapt the mesh resolution to the local TBL thickness, δ. This is achieved through unstructured mesh generation based on an a-priori estimate of δ over the wall surface. For the flat-plate case, this estimate is obtained by the application of a power law for the growth of the thickness along the plate. For a complex geometry, it can be obtained by a preliminary RANS simulation of the flow.

The CFD framework employed is a second-order accurate finite volume discretisation, on meshes consisting of arbitrary polyhedral cells. The mesh-cell topology has an important impact on the accuracy of WMLES, and the requirements on mesh quality are high. The conducted simulations show that the here proposed meshing strategy results in meshes adhering to these requirements. With respect to the cell topology, two options are considered: a hex-dominant mesh and a polyhedral. Both are shown to lead to accurate results. Furthermore, the procedure for velocity sampling for the wall model is emphasised. The conventional approach, see e.g. [6], employs the wall-adjacent cell layer for this purpose. Here, this is compared to sampling velocity further away from the wall, and it is shown that this leads to a significant improvement of the predictions.

The article is structured as follows. Section 2 details the employed computational fluid dynamics methods. In Section 3 the conducted numerical experiments are presented, including the description of the meshing strategy, the case set-up, and the results. Section 4 summarises the work and gives concluding remarks.

2 COMPUTATIONAL FLUID DYNAMICS METHODS

The LES equations are obtained by applying a low-pass filter to the Navier-Stokes equations. Assuming incompressible flow and commutativity between filtering and derivation, the filtered equations are as follows.

$$\begin{aligned} \frac{\partial \overline{v}_i}{\partial t} + \frac{\partial}{\partial x_j}(\overline{v}_i \overline{v}_j) &= -\frac{1}{\rho}\frac{\partial \overline{p}}{\partial x_i} + \nu\left(\frac{\partial \overline{v}_i}{\partial x_j} + \frac{\partial \overline{v}_j}{\partial x_i}\right) + \frac{\partial \tau_{ij}^{\text{sgs}}}{\partial x_j}, \quad (i = 1, 2, 3) \qquad (1) \\ \frac{\partial \overline{v}_j}{\partial x_j} &= 0. \end{aligned}$$

Here, the overbar is used to indicate that the variable is filtered, v_i are the components of velocity, p is the pressure, ρ is the density of the fluid, and ν is its kinematic viscosity. The term τ_{ij}^{sgs} is the subgrid stress tensor and, in on order to close the system of equations, it has to be modelled. In this work, the WALE model [17] is employed to that end.

All computations have been performed using the open-source general-purpose CFD software `OpenFOAM`. It employs the collocated finite volume method for discretisation and

supports arbitrary polyhedral cells. Interpolation is required to obtain the values of the unknowns at the cells' face centres. To that end, linear interpolation is used when addressing the diffusive terms in (1), and the LUST scheme [29, 15] is adopted for the convective term. Both schemes are second-order accurate. For discretisation in time, a backward-differencing scheme is used, also second-order accurate, see [9]. The governing equations (1) are solved in a segregated manner, using the PISO algorithm [8]. Three pressure-correction steps are performed at each time-step.

An algebraic wall-stress model based on Spalding's law [28] is employed. The formulation of the model within the framework of collocated finite volume discretisation is discussed in detail in [14]. Implementation using `OpenFOAM` technology[1] is presented in [16]. The model attempts to account for the dynamics of the inner layer by enforcing the correct local value of the wall shear stress at each face centre of the wall patch. This is done in three steps. i) Sampling the value of the wall-parallel velocity from a cell centre at a wall-normal distance, h, from the wall. An individual value of h is set for each wall face prior to the simulation. ii) Computing the value of the wall shear stress using the sampled velocity and Spalding's law. The law acts as a non-linear equation, with the wall shear stress being the unknown, and is solved using the Newton-Raphson method. iii) Enforcing the computed wall shear stress at the wall. This is done by adding the appropriate amount of subgrid viscosity at the wall face, see [14] for details.

3 NUMERICAL EXPERIMENTS

3.1 Case set-up

This section summarises the set-up of the simulations, excluding the used meshes, which are discussed in the section below. The triple x, y, z will be from here on used to denote the streamwise, wall-normal, and spanwise directions, respectively. A summary of the simulation parameters is given in Table 1.

The computational domain is a box of size $L_x = 2$ m, $L_y = 1$ m, $L_z = 0.2$ m along the respective coordinate axes. The two latter dimensions should be compared with the maximum value of the thickness of the TBL, $\delta_{\max} \approx 0.03$ m, giving $L_y/\delta_{\max} \approx 33.3$ and $L_z/\delta_{\max} \approx 6.7$. These values are large enough to avoid loss of accuracy due to the imposed boundary conditions, which are as follows.

At the wall ($y = 0$), the no-slip condition is applied. At the inlet ($x = 0$) a uniform velocity, $U_0 = 20.4$ m/s, is prescribed. At the outlet ($x = L_x$), the pressure is prescribed to be zero and a Neumann condition is used for the velocity. The top boundary is treated as a symmetry plane. Finally, periodic boundary conditions are used on the left and right sides of the domain ($z = 0$ and $z = L_z$).

In order to facilitate the transition of the boundary layer to fully turbulent state, numerical tripping is introduced. This is done by adding a source term to the momentum equation, which is active only within a short strip of cells located shortly downstream of the inlet ($x = 0.1$) and the magnitude of which is randomised in space and time. The strip stretches across the whole domain in the spanwise direction, but is limited to 20 cm

[1]Source code available at `https://bitbucket.org/lesituu/libwallmodelledles`.

and 3 mm in the streamwise and wall-normal directions, respectively.

After initial transients are removed from the domain, averaging in time is performed during a period of 0.245 s, which corresponds to about 2.5 flow-through times, defined as $T_{ft} = L_x/U_0$. The time-steps of the simulations are 4 μs and 5 μs for the polyhedral and paved mesh (see below), respectively.

Two simulations on each mesh are performed, which differ in the way the sampling point of the wall model is chosen. In one simulation, the centre of the wall-adjacent cell is used for sampling. In the other, the centre of the third consecutive off-the-wall cell is used instead.

Table 1: Simulation parameters.

Quantity	**Notation**	**Value**
Length of the domain	L_x	2 m
Height of the domain	L_y	1 m
Width of the domain	L_z	0.2 m
Free-stream velocity	U_0	20.4 m
Kinematic viscosity	ν	$1.65 \cdot 10^{-5}$ m$^2/s$
Flow-through time	T_{ft}	≈ 0.1 s
Time-averaging period	T_{avrg}	≈ 0.245 s
Time-step, paved mesh	Δt_{paved}	$5 \cdot 10^{-6}$ s
Time-step, polyhedral mesh	Δt_{poly}	$4 \cdot 10^{-6}$ s

3.2 Meshing strategy

This section discusses the two computational meshes used in the study. Both meshes are constructed using the same strategy, which relies on a-priori knowledge of the thickness of the boundary layer, δ, as a function of x. For the TBL, $\delta(x)$ can be estimated using a power-law relation [23]. It was considered that the boundary layer achieved fully turbulent state at $x_0 = 0.4$. Consequently, for $x > x_0$, δ is computed using the power law estimate, and upstream a constant value of $\delta = \delta(x_0)$ is employed.

The domain to be meshed can be roughly divided into two regions: the one occupied by the boundary layer and the one with the free stream. The goal is to generate a high-quality unstructured mesh for the boundary layer region, with the resolution of the mesh adapted to the local value of $\delta(x)$. The free stream region can then be covered with significantly coarser cells.

The meshing is performed in three steps. First, the surface of the wall boundary is meshed. This is done in such a way, that the average distance between the cell centres, d, is maintained as a specified fraction of the local value of $\delta(x)$. In particular, here $\delta/d \approx 15.5$ is employed. This is consistent with recommendations for the resolution of a WMLES mesh found in the literature [27, 11]. Note that since δ grows in the streamwise direction, the density of the surface mesh is highest near the inlet and gradually decreases

towards the outlet, see Figure 1. The same figure also shows the average cell size in wall-units, d^+. Near the inlet, d^+ is ≈ 25 and reaches ≈ 80 at the outlet.

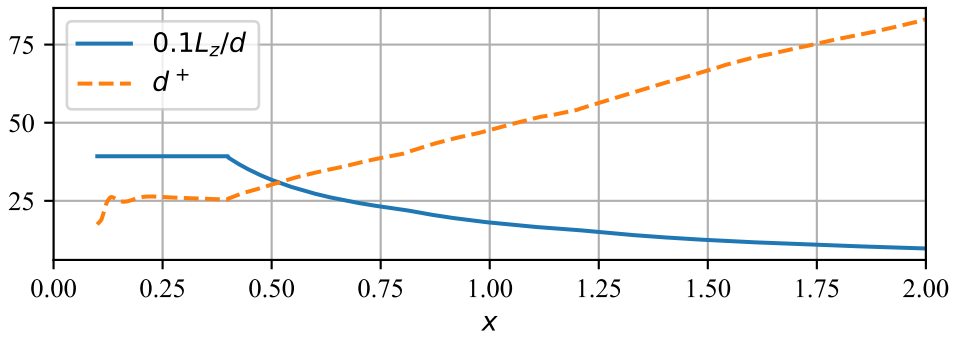

Figure 1: The number of cells across the spanwise direction of the plate (blue line), and the size of cells in wall units, d^+ (orange).

The second step in the meshing strategy is to extrude the generated surface mesh in the wall-normal direction. The extrusion is performed by building layers. A total number of 16 layers is built, and the thickness of each layer at a given streamwise location is set in such a way that the height of the extruded mesh matches the local value of $\delta(x)$. As a result, the wall-normal resolution of the grid with respect to $\delta(x)$ matches that of the surface mesh.

As a final step, the rest of the domain is meshed using a significantly coarser mesh, with rapid increase of the cell size in the wall-normal direction. The result of applying this meshing strategy is shown in Figure 2.

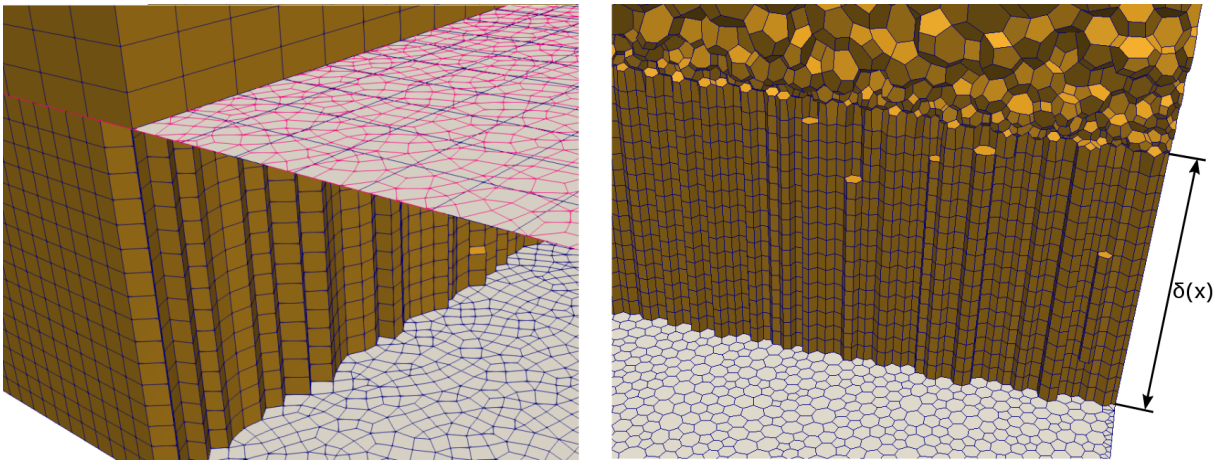

Figure 2: Structure of the two meshes used in the simulations: paved (left) and polyhedral (right). The surface mesh, the extruded layers, and the coarse mesh above the TBL are visualised. For the paved mesh, the AMI is also shown.

The two constructed meshes differ in the topology of the cells that constitute them. The first mesh, referred to "paved" below, uses a quad-dominant surface mesh, see the

left plot in Figure 2. Consequently, the extruded layers are hex-dominant. The region above the TBL is meshed with a structured hexahedral mesh. In order to connect it to the layers extruded from the surface, a so-called arbitrary mesh interface (AMI) is used, which allows to couple two non-conforming regions of a mesh across a defined surface. The second mesh, referred to as "polyhedral", uses polygons to discretise the wall-surface, see the right plot in Figure 2. The polygons are obtained as a dual of a triangulation. Above δ, an unstructured polyhedral mesh is used, alleviating the need for an AMI.

The sizes of the constructed paved and polyhedral meshes are $N_{\text{paved}} \approx 15.5 \cdot 10^6$ and $N_{\text{poly}} \approx 14.4 \cdot 10^6$, respectively. Considering only the region occupied by the TBL brings the figures down to $N^{\text{TBL}}_{\text{paved}} \approx 14.7 \cdot 10^6$ and $N^{\text{TBL}}_{\text{poly}} \approx 12.9 \cdot 10^6$. It is interesting to compare these mesh sizes to that required for a wall-resolved simulation of the same case. Consider a structured hexahedral mesh, with uniform cell sizes $\Delta x^+ = 20$ and $\Delta z^+ = 10$ in the wall-parallel directions, where the scaling is done with values of δ_ν taken at $x = x_0$. This results in 1000 cells across L_z and 5000 cells across L_x. If $\delta(x)$ is discretised with 50 cells, the number of cells in the TBL region amounts to $250 \cdot 10^6$, which is 17 times larger than the paved WMLES mesh. Note that adapting Δx^+ to the local value of δ_ν would not result in a significant change in the estimate, because δ_ν grows only by a factor of ≈ 1.15 over the interval $[x_0, L_x]$. By comparison, δ grows by a factor of ≈ 4.

3.3 Results

This section presents the simulation results, a selection of which is also made available online[2]. Attention is first drawn to Figure 3 visualising the resolved structures in the TBL. The effect of the numerical tripping is clearly seen, the first structures appearing in the box where the tripping is active. The growth of the TBL is evident and, correspondingly, the growth in the size of the largest resolved structures.

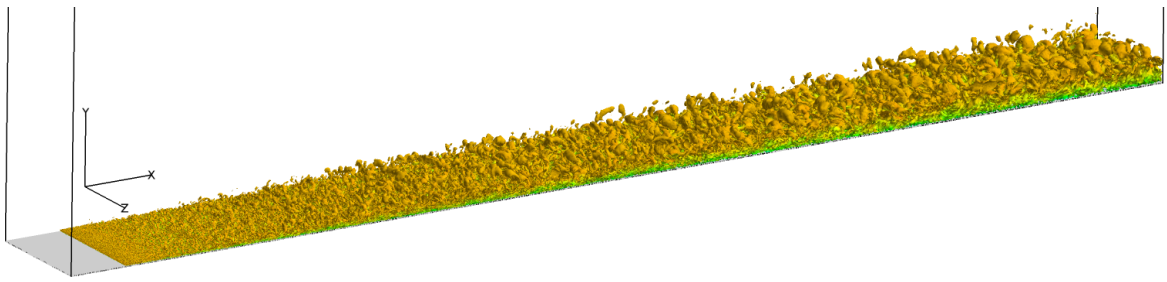

Figure 3: Resolved turbulent structures visualised by an iso-surface of the second invariant of the velocity gradient, coloured by streamwise velocity.

This growth is further quantified in Figure 4, which shows the development of the momentum thickness-based Re-number as a function of the streamwise coordinate. In addition to the simulation results, an estimate obtained from a power-law proposed in [23] is shown. All four simulations show acceptable agreement with the estimate, but the

[2]DOI: `10.6084/m9.figshare.6061298`

simulation employing the polyhedral mesh and sampling from the third off-the-wall cell clearly performs best.

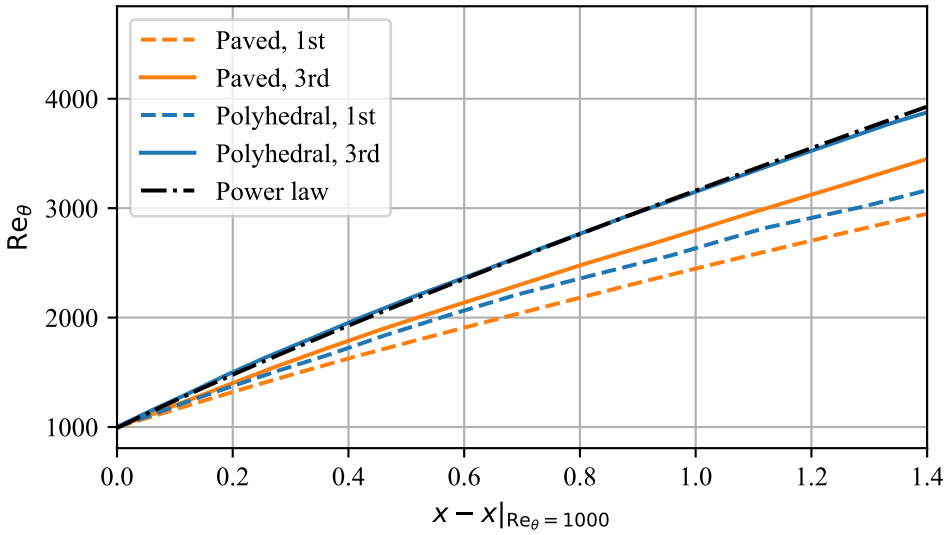

Figure 4: Development of the momentum thickness based Reynolds number, Re_θ.

The skin friction coefficient, c_f, is shown as a function of Re_θ in Figure 5. DNS data from [24] and a power-law estimate from [23] are used as reference. After a short transient period, all four curves behave similarly to the benchmark data. However, the values obtained from the two simulations employing sampling from the third off-the-wall cell are in significantly better agreement with the reference.

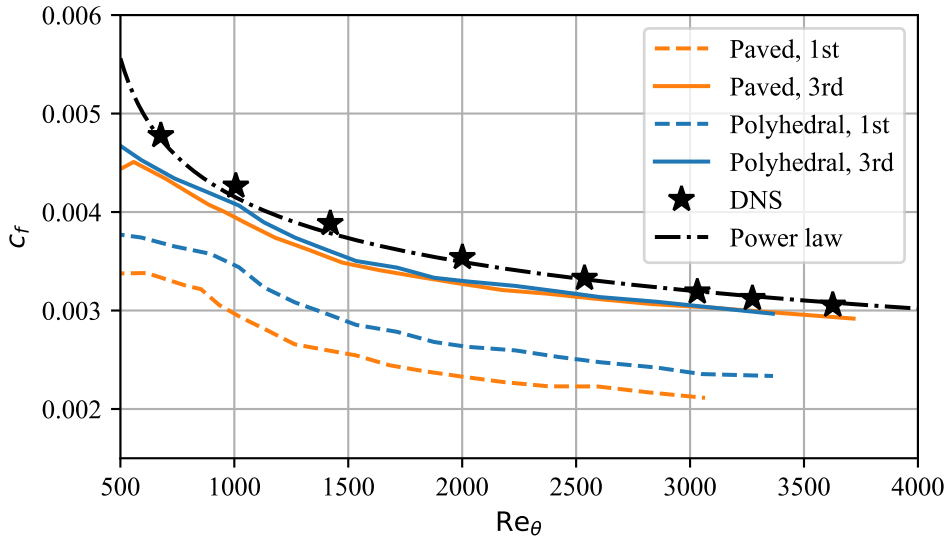

Figure 5: Development of the skin friction coefficient, c_f.

The under-prediction in c_f exhibited by the simulations using sampling from the wall-

adjacent cell entails that they under-predict the mean wall shear stress, $\langle \tau_w \rangle$ (by definition of c_f). This is further demonstrated in Figure 6, which shows inner-scaled profiles of the mean streamwise velocity for selected values of Re_θ. DNS data [24] is used as reference. It is observed that all four simulations predict similarly-shaped profiles, but those from the simulations with sampling from the wall-adjacent cell are shifted along the ordinate. Thus the value of $\langle u_\tau \rangle = \sqrt{\langle \tau_w \rangle / \rho}$ in these simulations is under-predicted. The overall agreement of the profiles with DNS data is good, although they exhibit a very pronounced log-layer which is not present at these relatively low Re-numbers. The best accuracy is achieved with the paved grid, using sampling from the third off-the-wall cell.

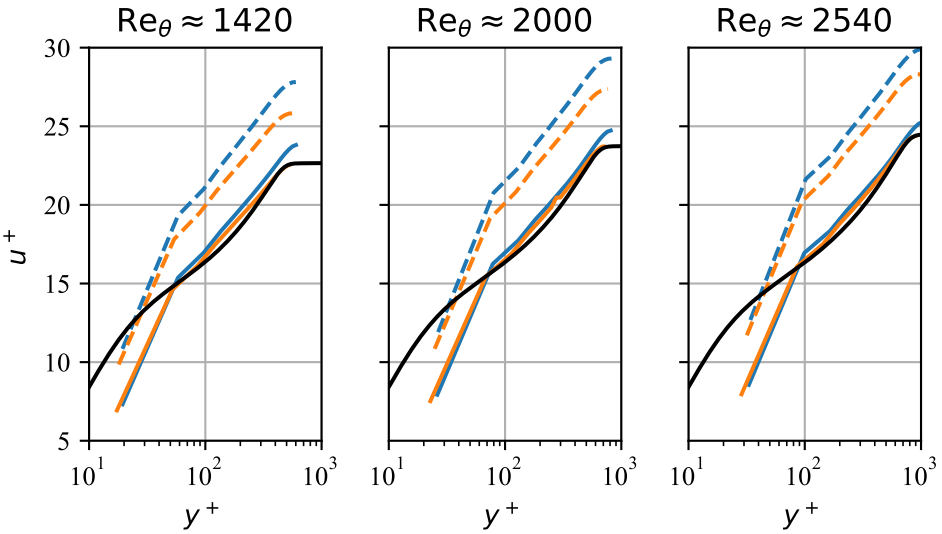

Figure 6: Profiles of the mean streamwise velocity at three different downstream locations, corresponding to $\mathrm{Re}_\theta \approx 1420$, 2000, and 2540, respectively. Black solid lines show DNS data [24], other lines are as in Figure 5.

Figure 7 shows the profiles of the Reynolds stresses for three selected values of Re_θ. The level of agreement with DNS data is acceptable and typical of WMLES. The observed errors, such as the over-prediction and shift away from the wall of the peak value of u^{rms} are common for LES on coarse meshes in general [2]. Arguably, the results obtained with the paved mesh are slightly better than those obtained with the polyhedral.

4 CONCLUSIONS

Results from WMLES of a zero pressure gradient TBL over a flat plate are presented. The simulations are performed on unstructured meshes of two types: hex-dominant (paved) and polyhedral. The meshes are carefully constructed to preserve the density of the mesh with respect to the thickness of the TBL. The quality of the meshes is high enough to allow using second-order accurate schemes for discretising the governing equations. Further, two locations for sampling velocity values for the employed algebraic wall model are tested: the wall-adjacent cell and the third consecutive off-the-wall cell.

The results show convincingly that the employed meshing strategy, in conjunction with

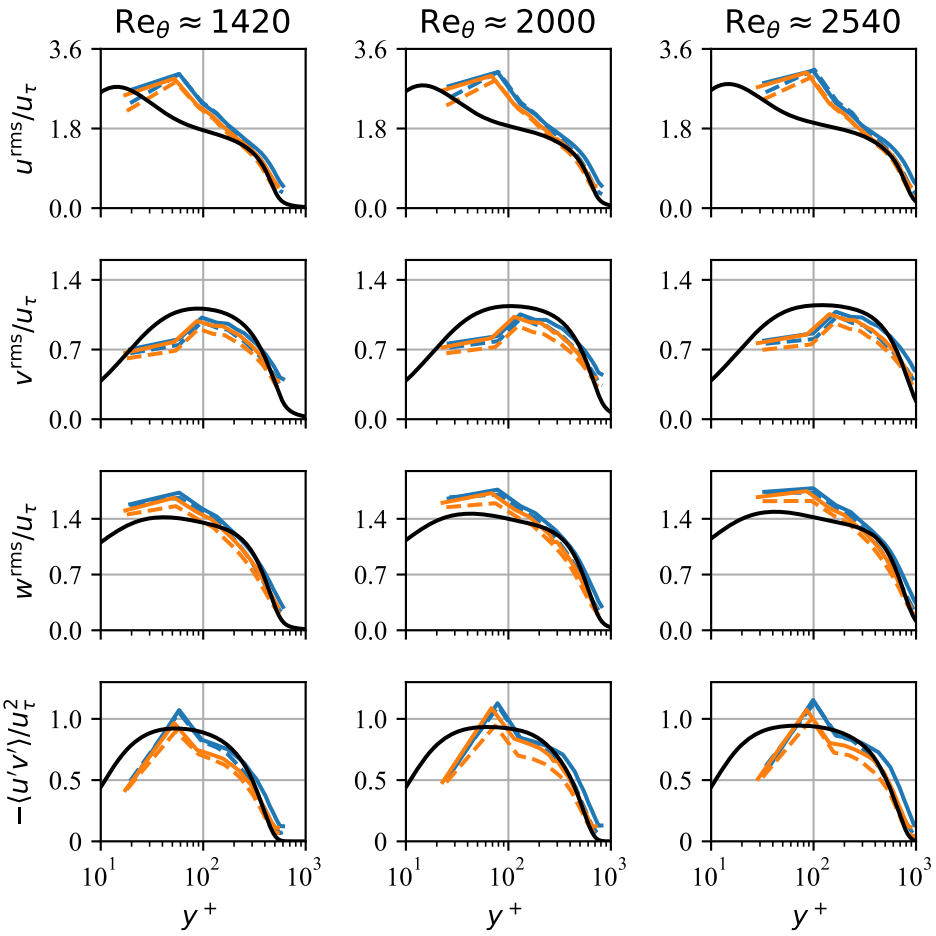

Figure 7: Profiles of the Reynolds stresses at three different downstream locations, corresponding to $\mathrm{Re}_\theta \approx 1420$, 2000, and 2540, respectively. Black solid lines show DNS data [24], other lines are as in Figure 5.

the employed numerical methods, is suitable for WMLES. It is emphasised that while the geometry of the considered flow is simple, the developed methodology is fully applicable to complex geometries. Using both the paved and the polyhedral mesh led to an overall similar level of accuracy of the solution. The polyhedral grid was superior in predicting the values of Re_θ and c_f (see Figures 4 and 5), but the paved grid gave slightly better predictions of the mean streamwise velocity and the Reynolds stresses (Figures 6 and 7).

Using the wall-adjacent cell is shown to lead to an under-prediction of the mean wall shear stress by $\approx 20\%$. In line with what has previously been reported in the literature [10, 12, 7, 16], moving the sampling point further away from the wall results in a significant improvement. In particular, no log-layer mismatch is observed for the mean streamwise velocity, as compared to the DNS data.

ACKNOWLEDGEMENTS

The study was supported by the Grant No 621-2012-372 from the Swedish Research Council.

REFERENCES

[1] D. E. Aljure, J. Calafell, A. Baez, and A. Oliva. Flow over a realistic car model: Wall modeled large eddy simulations assessment and unsteady effects. *Journal of Wind Engineering and Industrial Aerodynamics*, 174:225–240, 2018.

[2] H. J. Bae, A. Lozano-Durán, S. T. Bose, and P. Moin. Turbulence intensities in large-eddy simulation of wall-bounded flows. *Physical Review Fluids*, 3:014610, 2018.

[3] S. T. Bose and P. Moin. A dynamic slip boundary condition for wall-modeled large-eddy simulation. *Physics of Fluids*, 26(015104):1–18, 2014.

[4] S. T. Bose and G. I. Park. Wall-modeled large-eddy simulation for complex turbulent flows. *Ann. Rev. Fluid Mech.*, 50:535–561, 2018.

[5] L. Davidson, D. Cokljat, J. Fröhlich, , M. A. Leschziner, C. Mellen, and W. Rodi, editors. *LESFOIL: Large-eddy simulation of flow around a high-lift airfoil*, chapter Task 2: Near-wall models. Notes on Numerical Fluid Mechanics and Multidisciplinary Design. Springer, 2003.

[6] E. de Villiers. *The potential of large-eddy simulation for the modeling of wall-bounded flows*. PhD thesis, The Imperial College of Science, Technology and Medicine, 2006.

[7] A. Frère, C. C. de Wiart, K. Hillewaert, P. Chatelain, and G. Winckelmans. Application of wall-models to discontinuous Galerkin LES. *Physics of Fluids*, 29:085111, 2017.

[8] R. I. Issa. Solution of the implicitly discretised fluid flow equations by operator-splitting. *Journal of Computational Physics*, 62(1):40–65, 1986.

[9] H. Jasak. *Error Analysis and Estimation for the Finite Volume Method with Applications to Fluid Flows*. PhD thesis, The Imperial College of Science, Technology and Medicine, 1996.

[10] S. Kawai and J. Larsson. Wall-modeling in large eddy simulation: Length scales, grid resolution, and accuracy. *Physics of Fluids*, 24(1):015105, 2012.

[11] J. Larsson, S. Kawai, J. Bodart, and I. Bermejo-Moreno. Large eddy simulation with modeled wall-stress: recent progress and future directions. *Mechanical Engineering Reviews*, 3(1):1–23, 2016.

[12] J. Lee, M. Cho, and H. Choi. Large eddy simulations of turbulent channel and boundary layer flows at high Reynolds number with mean wall shear stress boundary condition. *Physics of Fluids*, 25:110808, 2013.

[13] M. Liefvendahl and C. Fureby. Grid requirements for LES of ship hydrodynamics in model and full scale. *Ocean Engineering*, 143:259–268, 2017.

[14] M. Liefvendahl, T. Mukha, and S. Rezaeiravesh. Formulation of a wall model for LES in a collocated finite-volume framework. Technical Report 2017-001, Uppsala University, Department of Information Technology, 2017.

[15] J. Martínez, F. Piscaglia, A. Montorfano, A. Onorati, and S. M. Aithal. Influence of spatial discretization schemes on accuracy of explicit LES: Canonical problems to engine-like geometries. *Computers and Fluids*, 117:62–78, 2015.

[16] T. Mukha, S. Rezaeiravesh, and M. Liefvendahl. An OpenFOAM library for wall-modelled Large-Eddy Simulation. In *12th OpenFOAM Workshop*, 2017.

[17] F. Nicoud and J Baggett. On the use of the optimal control theory for deriving wall models for LES. *Annual Research Briefs, Center for Turbulence Research, Stanford University*, pages 329–341, 1999.

[18] C. Pantano, D. I. Pullin, P. E. Dimtakis, and G. Matheou. LES approach for high Reynolds number wall-bounded flows with application to turbulent channel flow. *J. Comp. Phys.*, 227:9271–9291, 2008.

[19] G. I. Park and P. Moin. An improved dynamic non-equilibrium wall-model for large-eddy simulation. *Physics of Fluids*, 26(015108):1–21, 2014.

[20] U. Piomelli. Wall-layer models for large-eddy simulations. *Progress in Aerospace Sciences*, 44:437–446, 2008.

[21] U. Piomelli and E. Balaras. Wall-layer models for large-eddy simulation. *Annual Review of Fluid Mechanics*, 34:349–374, 2002.

[22] U. Piomelli, J. Ferziger, P. Moin, and J. Kim. New approximate boundary conditions for large-eddy simulations of wall-bounded flows. *Physics of Fluids A*, 1(6):1061–1068, 1989.

[23] S. Rezaeiravesh, M. Liefvendahl, and C. Fureby. On grid resolution requirements for LES of wall-bounded flows. In *ECCOMAS Congress 2016, Crete, Greece*, 2016.

[24] P. Schlatter and R. Örlü. Assessment of direct numerical simulation data of turbulent boundary layers. *Journal of Fluid Mechanics*, 659:116–126, 2010.

[25] J. Slotnick, A. Khodadoust, J. Alonso, D. Darmofal, W. Gropp, E. Lau rie, and D. Marviplis. CFD vision 2030 study: A path to revolutionaty computational aero-sciences. *NASA Technical Report*, 2014-218178, 2014.

[26] P. R. Spalart. Detached-eddy simulation. *Annual Review of Fluid Mechanics*, 41:181–202, 2009.

[27] P. R. Spalart, W. H. Jou, M. Strelets, and S. R. Allmaras. Comments on the Feasibility of LES for Wings and on a Hybrid RANS/LES Approach. In *Advances in DNS/LES*, volume 1, pages 4–8, 1997.

[28] D. B. Spalding. A single formula for the "law of the wall". *Journal of Applied Mechanics*, 28(3):455–458, 1961.

[29] H. Weller. Controlling the computational modes of the arbitrarily structured C grid. *Monthly Weather Review*, 140(10):3220–3234, 2012.